Available online at www.sciencedirect.com

ScienceDirect

Physics Procedia 85 (2016) 20 – 26

Physics Procedia

EMRS Symposium: In situ studies of functional nano materials at large scale facilities: From model systems to applications, EMRS Spring Meeting

Graphitization of activated carbons: a molecular-level investigation by INS, DRIFT, XRD and Raman techniques

Andrea Lazzarini[a,*], Andrea Piovano[b], Riccardo Pellegrini[c], Giovanni Agostini[d], Svemir Rudić[e], Carlo Lamberti[a,f] and Elena Groppo[a]

[a]*Department of Chemistry, NIS Centre and INSTM, University of Turin, Via Giuria 7, Turin, I–10125, Italy.*
[b]*Institut Laue-Langevin (ILL), 71 avenue des Martyrs, 38000 Grenoble, France.*
[c]*Chimet SpA - Catalyst Division, Via di Pescaiola 74, Viciomaggio Arezzo, I-52041, Italy.*
[d]*European Synchrotron Radiation Facility (ESRF), 71 avenue des Martyrs, 38000 Grenoble, France.*
[e]*ISIS Facility, Rutherford Appleton Laboratory, Chilton, Didcot, Oxfordshire, OX11 0QX, UK.*
[f]*Southern Federal University, Zorge street 5, 344090 Rostov-on-Don, Russia.*

Abstract

The effect of a graphitization treatment on the phyisico-chemical properties of an activated carbon have been studied by means of multi-technical approach. Inelastic neutron scattering and DRIFT spectroscopy revealed the modifications occurring at the material borders, involving H-containing species and O-containing functional groups. Information on the structural modifications were obtained by means of Raman spectroscopy and X-Ray Powder Diffraction.

Peer-review under responsibility of the organizing committee of the EMRS Spring Meeting 2016

Keywords: Activated carbons; Inelastic Neutron Scattering; Multi-technical Approach; Spectroscopy; Graphitization.

1. Introduction

Activated carbons are industrially relevant materials having large application in catalysis, where they are extensively employed as supports for noble metal nanoparticles. They may have mineral origin (derived from peat)

* Corresponding author. Tel.: +39 011 670 8375.
E-mail address: andrea.lazzarini@unito.it

Peer-review under responsibility of the organizing committee of the EMRS Spring Meeting 2016
doi:10.1016/j.phpro.2016.11.076

or can be produced by pyrolysis of organic biomasses, mainly wood and coconut shells [1-7]. Depending on the activation procedure, they are composed of a significant amount of graphite-like "structural units" (sp^2 domains) of different size. The activation consists of a high temperature thermal treatment in presence of gaseous H_2O or H_3PO_4. This process is responsible for the formation of pores of different size and shapes and hence to the development of large surface areas (up to 1500 m^2/g). The activation procedure also affects the carbon structure at a micro- and nanoscale (e.g. the dimension of the sp^2 domains), as well as the surface chemistry (e.g. activation in presence of phosphoric acid usually introduces oxygen-containing surface groups). Recently, we have demonstrated that there is a strong relationship between the physico-chemical properties of the activated carbons and the final performances of the carbon-supported catalysts [8], in terms of long-term activity, selectivity and stability.

Post-activation treatments are valuable methods to tune the properties of activated carbons, and hence those of the corresponding catalyst. In this work, we investigate the structural and surface changes occurring in a chemically activated carbon upon a well-established procedure which is called *graphitization* [9-14], consisting in a thermal treatment in inert atmosphere. The purpose of the treatment is to induce a gradual regularization of the structure of the activated carbon. This process has been monitored at a nano-scale level by coupling four different techniques: Inelastic Neutron Scattering (INS), Diffuse Reflectance IR spectroscopy (DRIFT), Raman spectroscopy and X-Ray Powder Diffraction (XRPD).

1) INS has been extensively used in the past for deep studies on carbon-based materials and related supported nanoparticles catalysts [15-21]. For these materials, it is sensitive mainly to the vibrations of hydrogen-containing species (whose incoherent scattering length is more than one order of magnitude higher with respect to all other elements), which are the majority of the terminations present at the edges of the sp^2 domains. Differently from light-based vibrational spectroscopies, INS allows observation of all the H-related vibrations without selection rules, giving a response that is proportional to the quantity of the corresponding chemical species.
2) DRIFT and Raman spectroscopy are complementary to INS in that they are sensitive to vibrations associated respectively to changes in dipole moment or in polarizability of the specific chemical species. Both techniques have been widely used in the past to characterize the surface species of activated carbons [22-29] and related supported metal nanoparticles catalysts [30, 31]. In particular, structural information on the bulk of carbon materials are mainly given by Raman technique; with DRIFT, instead, it is possible to obtain directly information about the surface species (such as oxygen-containing functional groups) [8].
3) XRPD provides basic information on the structure of carbons, and in particular on the extension of the regular sp^2 domains.

The combined use of these techniques allowed us to fully characterize the structural and surface changes induced on our carbon by the graphitization process.

2. Experimental section

2.1. Materials

The starting activated carbon is the same as the one deeply studied in our previous work [8], named as C_{Chemi}, and was provided by Chimet S.p.A. [32]. Briefly, it is a carbon of wood origin, chemically activated with H_3PO_4 at high temperature, and displaying a specific surface area of 1500 m^2/g. C_{Chemi} was subjected to two graphitization treatments, consisting of a heating in N_2 atmosphere (at a rate of 10 °C/min) up to T_{max}, followed by an isotherm of 30 minutes at T_{max}, with T_{max} = 350 °C and 750 °C. The two samples will be named hereafter C_{350} and C_{750}, respectively.

2.2. Methods

Inelastic Neutron Scattering. INS spectra were collected by TOSCA neutron spectrometer at the ISIS Neutron and Muon Source (Rutherford Appleton Laboratory, UK) [33]. The samples were treated under dynamic vacuum at 150 °C for several hours before the measurements, with the aim to desorb the water physisorbed on samples surface. Afterwards, they were placed inside an aluminum foil envelope (to avoid the loss of neutron-activated radioactive

powders) and inserted into an In-wire sealed Al sampleholder. All the samples were manipulated inside a glove-box, in order to avoid contamination by moisture. The measurement cell was positioned in a duplex CCR cryostat and INS spectra were collected at 20 K. Each measurement was performed by integrating for 1500 μA of proton current. Data were collected either in forward or in backward scattering detectors and were analyzed by using Mantid software [34], with no degradation in resolution. The large beam size (40×40 mm^2) allowed us to measure sample quantities of the order of grams. Since INS signal intensity for a chemical species is proportional to the total amount irradiated by the neutron beam, the spectra were normalized with respect to sample mass (C_{Chemi} = 7.6502 g; C_{350} = 5.6388 g; C_{750} = 7.3520 g) and incoming proton current, allowing us to perform a quantitative comparison between the samples measured.

DRIFT spectroscopy. DRIFT spectra were acquired by using a Nicolet 6700 instrument equipped with a ThermoFisher Smart accessory and a MCT detector. They were collected by averaging 1024 spectra with a spectral resolution of 4 cm^{-1}. The samples were measured in powdered form in air, without any dilution in KBr. The spectra, collected in diffuse reflectance mode, were successively converted in Kubelka-Munk units (K.M.).

X-Ray Powder Diffraction. XRPD patterns were collected using a PANalytical PW3050/60 X'Pert PRO MPD diffractometer in Debye-Scherrer configuration, having a Cu anode as X-rays source and a Ni filter to attenuate Cu K_β line. The beam was focused with a PW3152/63 X-ray mirror (λ = 1.5409 Å). The measurements were performed by using a 0.5 mm glass capillary. The average dimension (L_a) of the crystalline domains was calculated by applying the Scherrer equation, $L_a = K\lambda/\beta cos(\theta_{Bragg})$, where K is a non-dimensional shape factor (usually fixed to 0.9) [35], λ is the wavelength of the Cu K_α radiation (1.541 Å), and β is the FWHM (in 2θ value) of the (100) and (111) diffraction peaks.

Raman spectroscopy. Raman spectroscopy was performed with a Renishaw inVia Raman microscope, using an excitation radiation having λ = 514 nm. The power of the laser was posed equal to 0.5% of the maximum power, in order to avoid beam damage of the samples. Backscattered light coming from the sample was dispersed and monochromatized by using a 1800 lines/mm grating and simultaneously recorded with a CCD camera; the magnification of the microscope optics for the collection was set at 20 ×. The final spectra were obtained by averaging 20 acquisitions (50 s per each acquisition).

3. Results and discussion

3.1. Surface characterization

Fig.1a shows the INS spectra of C_{Chemi} (black), C_{350} (orange) and C_{750} (red) samples. The intensity of each band is proportionally related to the total amount of the corresponding species in the sample: this is possible because the spectra were previously normalized to the sample mass and to the proton current of the source. Each absorption band is related to a vibrational mode involving a significant displacement of a hydrogen atom, because hydrogen incoherent scattering length for neutrons is one order of magnitude larger than those of all the other elements. The INS spectrum of C_{Chemi} has been analyzed in detail in our previous works [8, 21]. Briefly: 1) the band at 3060 cm^{-1} is due to ν(C-H) of the aromatic moieties; 2) the broad band centered at 1200 cm^{-1} and the ones in the 800 – 1000 cm^{-1} region are assigned to the in-plane and out-of-plane C-H bending modes of hydrogen atoms at aromatic rings edges; and 3) the weak band in the 700 - 400 cm^{-1} region can be mainly ascribed to C-C torsion modes at the edges of the sp^2 platelets, causing a consequent perturbation of the hydrogen atoms (riding vibrations). The INS spectrum of C_{350} is the same as C_{Chemi}, indicating that the treatment at 350 °C does not affect the H terminations. In contrast, the spectrum of C_{750} shows a loss of intensity in the overall spectral region, which suggests that the amount of the H terminations is almost half of those present in C_{Chemi}. Going into deeper details, the band at 952 cm^{-1}, ascribed to C–H out-of-plane bending modes of species at irregular borders of the sp^2 domains, is the most affected by the thermal treatment. This observation provides evidence that during the graphitization processes the relative fraction of irregular borders at the sp^2 domains decreases in favor of the regular ones.

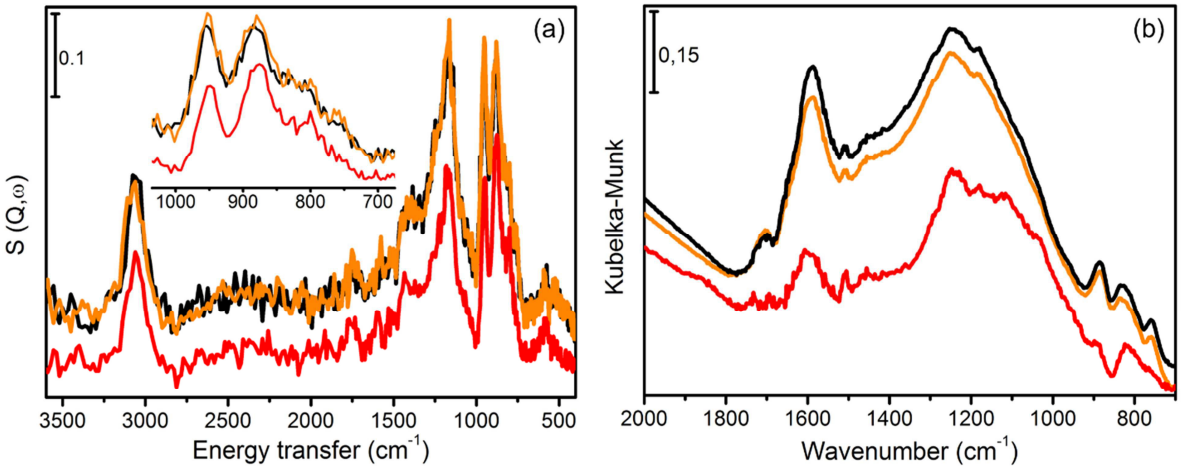

Fig.1. (a) INS spectra of C_{Chemi} (black curve), C_{350} (orange curve) and C_{750} (red curve), normalized by the incoming proton current and the sample mass. Inset shows a magnification of the 1050 – 650 cm^{-1} range. (b) DRIFT spectra of C_{Chemi} (black curve), C_{350} (orange curve) and C_{750} (red curve) in the 2000 – 700 cm^{-1} spectral region.

The DRIFT spectra of the same samples are shown in Fig.1b. As discussed in our previous work, the spectrum of C_{Chemi} is dominated by an absorption band centered at 1600 cm^{-1}, due to the ν(C=C) vibrations of carbon atoms belonging to the sp^2 rings, and by a very broad and intense signal in the 1300 – 1000 cm^{-1} region, which is mainly due to the C-C skeleton collective modes. In addition, the weak band at 1707 cm^{-1} is ascribed to the ν(C=O) modes of carboxyl groups, while the three bands at 880, 838 – 807 and 758 cm^{-1} are assigned to the C–H out-of-plane bending modes for an isolated hydrogen species (*solo*), and for two (*duo*) or three (*trio*) adjacent hydrogen species, respectively [36]. As for INS, the DRIFT spectrum of C_{350} (orange) is very similar to that of the parent sample (black). In contrast, the DRIFT spectrum on C_{750} is less intense in the overall spectral region and it does not show the ν(C=O) absorption band at 1707 cm^{-1}. Moreover, all the three bands related to C-H out-of-plane vibrations decrease in intensity, and only that at 880 cm^{-1} (*solo* species) remains well visible. Hence, the DRIFT data indicate that the graphitization process occurs at the expense of both the H-containing terminations (in agreement with INS) and of the oxygen-containing functional groups. The disappearance of functional groups characterized by a dipole moment explains the evident intensity decrease of the overall spectrum.

3.2. Structural characterization

The structural features of the three carbon samples were evaluated by using X-Ray Powder Diffraction technique. The XRPD patterns, shown in Fig. 2a, are very similar to each other and characterized by three very broad peaks corresponding to the (002), (100) and (111) reflections of graphite, proving that all the samples consist of small sp^2 platelets in agreement with literature data [8, 37-41]. Similarly to our previous work [8], we evaluated the lateral size (L_a) of the sp^2-ordered crystallites from the FWHM of the (100) and (111) diffraction peaks, by means of Scherrer equation. The results are summarized in Table 1. Although only a very small increase in L_a values are observed, these data may indicate a slow but progressive trend in the increase of lateral size of the sp^2 domains in the treated carbons. In our case of study, the evaluation of L_a obtained from the Scherrer equation should be considered only as semi-quantitative. Indeed, it has been observed that some highly oxidized graphites exhibit very small sp^2 domains and high the out-of-plane disorder but still preserves high correlation lengths parallel to the graphitic planes [42]. We are however far from those conditions.

Table 1. Calculated values of sp^2 platelets lateral dimensions (L_a) for C_{Chemi}, C_{350} and C_{750}.

Sample name	L_a (Å)	
C_{Chemi}	12.5 ± 0.5	[8]
C_{350}	12.9 ± 0.4	This work
C_{750}	13.0 ± 0.4	This work

The Raman spectra of C_{Chemi}, C_{350} and C_{750} are shown in Fig. 2b. They are dominated by two bands attributed to vibrations involving carbon atoms belonging to sp^2 rings of disordered microcrystalline domains. The band centered at 1605 cm^{-1} (G band, related to vibrational modes having E_{2g} symmetry) is assigned to the stretching of carbon atoms pairs of sp^2 domains (both in aromatic rings and conjugated chains) [3-5]. The band around 1350 cm^{-1} (D band, ascribed to lattice breathing mode having A_{1g} symmetry), is forbidden for non-defective graphite; however, it becomes Raman active whenever structural disorder is present [3-5, 43-45]. According to Tuinstra and Koenig [46], the relative intensity between these two signals, expressed as I(D)/I(G), should be strictly related with the structural disorder degree and hence with the size of the graphitic domains, following the law $I(D)/I(G) \propto L_a^{-1}$. However, according to Ferrari and Robertson [47], this relation loses validity when the lateral dimension of the sp^2 domains is below 2 nm, and the law transforms into $I(D)/I(G) \propto L_a^2$. This is the case for all the samples investigated in this work, as determined by XRPD (Table 1).

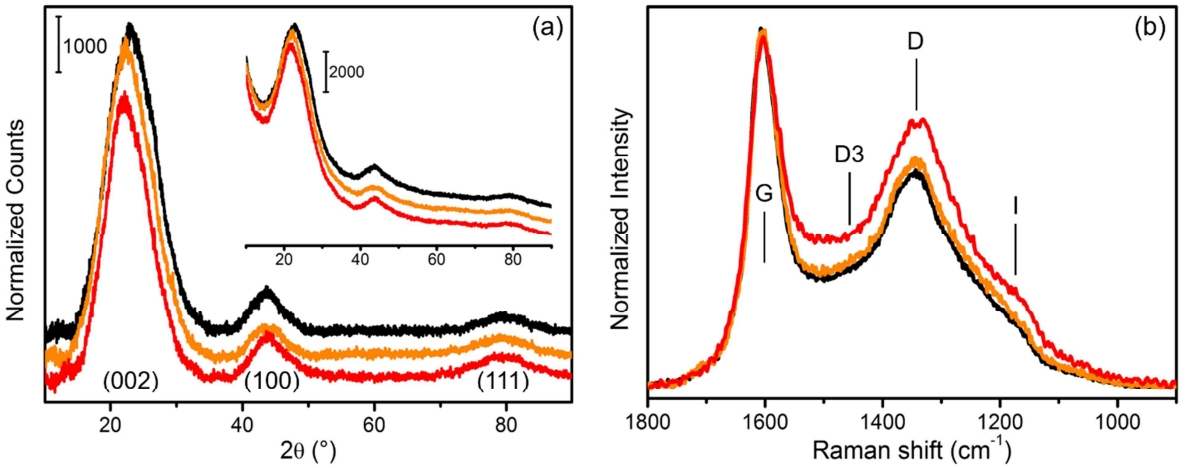

Fig. 2. (a) Area-normalized XRPD patterns of C_{Chemi} (black curve), C_{350} (orange curve) and C_{750} (red curve) samples after subtraction of the background. The inset shows the patterns as collected. All the spectra were shifted in order to facilitate visualization. (b) Raman spectra of C_{Chemi} (black curve), C_{350} (orange curve) and C_{750} (red curve) samples. Spectral intensity is normalized on 1600 cm^{-1} signal (G), in order to emphasise I(D)/I(G) ratio.

Table 2 reports the I(D)/I(G) ratios for all the samples. Only for C_{750} a slight increase in I(D)/I(G) is observed, which indicates a modification towards a more regular structure. In contrast, no changes are observed for the band at 1450 cm^{-1} (D3 band), ascribable to a random distribution of amorphous carbon in the interstitial position of the regular sp^2 platelets [48], neither for that at 1150 cm^{-1} (I band), due to the simultaneous presence of sp^2 phase (in the form of conjugated linear polyenes) and sp^3 phase [49]. Finally, in the spectrum of C_{750}, the weak band around 1700 cm^{-1}, related to C=O groups and present in the Raman spectrum of C_{Chemi}, disappears, according to what was observed by DRIFT spectroscopy [50].

Table 2. Calculated values of I(D)/I(G) ratio for C_{Chemi}, C_{350} and C_{750}. Intensities are intended as the area of the peak obtained after performing a signal deconvolution.

Sample name	I(D)/I(G)
C_{Chemi}	1.35 ± 0.31
C_{350}	1.40 ± 0.18
C_{750}	1.88 ± 0.10

4. Conclusions

The synergic application of INS, DRIFT, XRPD and Raman techniques allowed us to understand how the early stages of the graphitization process influence the structure and the surface properties of an activated carbon. The thermal treatment at 750 °C affects the oxygen- and hydrogen-containing terminations belonging to irregular borders of sp^2 platelets constituting the skeleton of the materials, but it is not able to enlarge consistently these graphitic domains. This effect is documented only for temperature values above 2000 °C in the case of classic thermal treatments in inert atmosphere [9-11] or for temperatures between 800 °C and 1000 °C in the case of catalytic graphitization [12-14]. However, since our work is set in order to correlate catalyst activity and support properties, the total graphitization of the support would have led to the complete loss of the functional groups necessary to have interaction between the support and the active phase, affecting negatively the catalyst performances. Operating in this way, we preserved the support from the total loss of effectiveness in supporting metal nanoparticles for catalytic applications; moreover, further investigations on the performances of the catalyst obtained by supporting the active phase on a graphitized support are already planned.

Acknowledgements

C. Lamberti is grateful for support from the Mega-grant of the Russian Federation Government to support scientific research at the Southern Federal University, No. 14.Y26.31.0001.

References

1. Ahmadpour, A. and D.D. Do, 1996. *The preparation of active carbons from coal by chemical and physical activation.* Carbon 34 (4): 471-479.
2. Girgis, B.S., S.S. Yunis, and A.M. Soliman, 2002. *Characteristics of activated carbon from peanut hulls in relation to conditions of preparation.* Materials Letters 57 (1): 164-172.
3. Henning, K.-D. and H. von Kienle, 2000 *Carbon, 5. Activated Carbon*, in *Ullmann's Encyclopedia of Industrial Chemistry*. Wiley-VCH Verlag GmbH & Co. KGaA: Weinheim, Germany.
4. Marsh, H. and F. Rodríguez-Reinoso, 2006 in *Activated Carbon*. Elsevier. p. 13.
5. Schlögl, R., 2008 *Carbons*, in *Handbook of Heterogeneous Catalysis*. Wiley-VCH Verlag GmbH & Co. KGaA: Weinheim, Germany.
6. Marsh, H. and P.L. Walker Jr, 1979. *The effects of impregnation of coal by alkali salts upon carbonization properties.* Fuel Processing Technology 2 (1): 61-75.
7. Marsh, H., et al., 1984. *Formation of active carbons from cokes using potassium hydroxide.* Carbon 22 (6): 603-611.
8. Lazzarini, A., et al., 2016. *A comprehensive approach to investigate the structural and surface properties of activated carbons and related Pd-based catalysts.* Catalysis Science & Technology 6 (13): 4910-4922.
9. Asaka, K., M. Karita, and Y. Saito, 2011. *Graphitization of amorphous carbon on a multiwall carbon nanotube surface by catalyst-free heating.* Applied Physics Letters 99 (9): 091907.
10. Ōya, A. and H. Marsh, 1982. *Phenomena of catalytic graphitization.* Journal of Materials Science 17: 309-322.
11. Fuertes, A.B. and S. Alvarez, 2004. *Graphitic mesoporous carbons synthesised through mesostructured silica templates.* Carbon 42 (15): 3049-3055.
12. Barbera, K., et al., 2014. *Low-temperature graphitization of amorphous carbon nanospheres.* Chinese Journal of Catalysis 35 (6): 869-876.
13. Sevilla, M. and A.B. Fuertes, 2006. *Catalytic graphitization of templated mesoporous carbons.* Carbon 44 (3): 468-474.
14. Zhai, D.Y., et al., 2011. *Porous graphitic carbons prepared by combining chemical activation with catalytic graphitization.* Carbon 49 (2): 725-729.
15. Albers, P.W., et al., 2002. *Inelastic neutron scattering study on the influence of after-treatments on different technical cokes of varying impurity level and their sp^2/sp^3 character.* Carbon 40 (9): 1549-1558.
16. Albers, P.W., et al., 2003. *Investigations of activated carbon catalyst supports from different natural sources.* Physical Chemistry Chemical

Physics 5 (9): 1941-1949.
17. Fillaux, F., et al., 1995. *Inelastic neutron scattering study of free proton dynamics in coal.* Journal of Non-Crystalline Solids 188 (1-2): 161-168.
18. Fillaux, F., et al., 1994. *Inelastic neutron-scattering study of the proton dynamics in carbons and coals.* Carbon 32 (7): 1325-1331.
19. Fillaux, F., et al., 1995. *Inelastic neutron-scattering study of the proton dynamics in coals.* Fuel 74 (6): 865-873.
20. Honeybone, P.J.R., et al., 1994. *Structural properties of amorphous hydrogenated carbon. II. An inelastic neutron-scattering study.* Physical Review B 50 (2): 839-845.
21. Piovano, A., et al., 2015. *Progress in the Characterization of the Surface Species in Activated Carbons by means of INS Spectroscopy Coupled with Detailed DFT Calculations.* Advances in Condensed Matter Physics 2015: 803267.
22. Mawhinney, D.B. and J.T. Yates Jr, 2001. *FTIR study of the oxidation of amorphous carbon by ozone at 300 K - Direct COOH formation.* Carbon 39 (8): 1167-1173.
23. Meldrum, B.J. and C.H. Rochester, 1990. *In situ infrared study of the surface oxidation of activated carbon in oxygen and carbon dioxide.* Journal of the Chemical Society, Faraday Transactions 86 (5): 861-865.
24. Meldrum, B.J. and C.H. Rochester, 1990. *In situ infrared study of the modification of the surface of activated carbon by ammonia, water and hydrogen.* Journal of the Chemical Society, Faraday Transactions 86 (10): 1881-1884.
25. Meldrum, B.J. and C.H. Rochester, 1990. *In situ infrared study of the surface oxidation of activated carbon dispersed in potassium bromide.* Journal of the Chemical Society, Faraday Transactions 86 (17): 2997-3002.
26. Meldrum, B.J. and C.H. Rochester, 1990. *Fourier-transform infrared study of surface species on carbon mixed with KBr and reacted with CO_2, O_2 and CO.* Journal of the Chemical Society, Faraday Transactions 86 (21): 3647-3652.
27. Moreno-Castilla, C., F. Carrasco-Marín, and A. Mueden, 1997. *The creation of acid carbon surfaces by treatment with $(NH_4)_2S_2O_8$.* Carbon 35 (10-11): 1619-1626.
28. Moreno-Castilla, C., et al., 1995. *Activated Carbon Surface Modifications by Nitric Acid, Hydrogen Peroxide, and Ammonium Peroxydisulfate Treatments.* Langmuir 11 (11): 4386-4392.
29. Moreno-Castilla, C., N.V. Lòpez-Ramòn, and F. Carrasco-Marín, 2000. *Changes in surface chemistry of activated carbons by wet oxidation.* Carbon 38 (14): 1995-2001.
30. Gokagac, G., J.M. Leger, and F. Hahn, 2003. *Behaviour of bimetallic Pt-Pd carbon-supported catalysts in methanol electrooxidation.* Zeitschrift Fur Naturforschung Section B-a Journal of Chemical Sciences 58 (5): 423-432.
31. Venter, J.J. and M.A. Vannice, 1989. *DRIFTS investigation of the decomposition of ruthenium clusters on carbon and the subsequent ruthenium carbon catalysts.* Inorganic Chemistry 28 (9): 1634-1644.
32. http://www.chimet.com/en/catalyst.
33. Colognesi, D., et al., 2002. *TOSCA neutron spectrometer: The final configuration.* Applied Physics a-Materials Science & Processing 74: S64-S66.
34. Arnold, O., et al., 2014. *Mantid-Data analysis and visualization package for neutron scattering and SR experiments.* Nuclear Instruments and Methods in Physics Research Section A: Accelerators, Spectrometers, Detectors and Associated Equipment 764: 156-166.
35. Pellegrini, R., et al., 2011. *0.5 wt.% Pd/C catalyst for purification of terephthalic acid: Irreversible deactivation in industrial plants.* Journal of Catalysis 280 (2): 150-160.
36. Centrone, A., et al., 2005. *Structure of new carbonaceous materials: The role of vibrational spectroscopy.* Carbon 43 (8): 1593-1609.
37. Fujimoto, H., 2003. *Theoretical X-ray scattering intensity of carbons with turbostratic stacking and AB stacking structures.* Carbon 41 (8): 1585-1592.
38. Houska, C.R. and B.E. Warren, 1954. *X-Ray Study of the Graphitization of Carbon Black.* Journal of Applied Physics 25 (12): 1503-1509.
39. Li, Z.Q., et al., 2007. *X-ray diffraction patterns of graphite and turbostratic carbon.* Carbon 45 (8): 1686-1695.
40. Shen, T.D., et al., 1996. *Structural disorder and phase transformation in graphite produced by ball milling.* Nanostructured Materials 7 (4): 393-399.
41. Zickler, G.A., et al., 2006. *A reconsideration of the relationship between the crystallite size La of carbons determined by X-ray diffraction and Raman spectroscopy.* Carbon 44 (15): 3239-3246.
42. Mauro, M., et al., 2012. *Chemically Reduced Graphite Oxide with Improved Shape Anisotropy.* Journal of Physical Chemistry C 116 (46): 24809-24813.
43. Castiglioni, C., M. Tommasini, and G. Zerbi, 2004. *Raman spectroscopy of polyconjugated molecules and materials: confinement effect in one and two dimensions.* Philosophical Transactions of the Royal Society of London A: Mathematical, Physical and Engineering Sciences 362 (1824): 2425-2459.
44. Ferrari, A.C., 2007. *Raman spectroscopy of graphene and graphite: Disorder, electron-phonon coupling, doping and nonadiabatic effects.* Solid State Communications 143 (1-2): 47-57.
45. Tommasini, M., et al., 2011. *A joint Raman and EPR spectroscopic study on ball-milled nanographites.* Chemical Physics Letters 516 (4-6): 220-224.
46. Tuinstra, F. and J.L. Koenig, 1970. *Raman Spectrum of Graphite.* The Journal of Chemical Physics 53 (3): 1126-1130.
47. Ferrari, A.C. and J. Robertson, 2000. *Interpretation of Raman spectra of disordered and amorphous carbon.* Physical Review B 61 (20): 14095-14107.
48. Jawhari, T., A. Roid, and J. Casado, 1995. *Raman spectroscopic characterization of some commercially available carbon black materials.* Carbon 33 (11): 1561-1565.
49. Ferrari, A.C. and J. Robertson, 2001. *Origin of the 1150-cm^{-1} Raman mode in nanocrystalline diamond.* Physical Review B 63 (12): 121405.
50. Lin-Vien, D., et al., 1991. *The Handbook of Infrared and Raman Characteristic Frequencies of Organic Molecules*. London, UK: Academic Press.